JACS JOURNAL OF THE AMERICAN CHEMICAL SOCIETY

ARTICLE

pubs.acs.org/JACS

Growth of Ge Nanofilms Using Electrochemical Atomic Layer Deposition, with a "Bait and Switch" Surface-Limited Reaction

Xuehai Liang, Qinghui Zhang, Marcus D. Lay, and John L. Stickney*

Department of Chemistry, The University of Georgia, Athens, Georgia 30602, United States

ABSTRACT: Ge nanofilms were deposited from aqueous solutions using the electrochemical analog of atomic layer deposition (ALD). Direct electrodeposition of Ge from an aqueous solution is self-limited to a few monolayers, depending on the pH. This report describes an E-ALD process for the growth of Ge films from aqueous solutions. The E-ALD cycle involved inducing a Ge atomic layer to deposit on a Te atomic layer formed on Ge, via underpotential deposition (UPD). The Te atomic layer was then reductively stripped from the deposit, leaving the Ge and completing the cycle. The Te atomic layer was bait for Ge deposition, after which the Te was switched out, reduced to a soluble telluride, leaving the Ge (one "bait and switch" cycle). Deposit thickness was a linear function of the number of cycles. Raman spectra indicated formation of an amorphous Ge film, consistent with the absence of a XRD pattern. Films were more stable and homogeneous when formed on Cu substrates, than on Au, due to a larger hydrogen overpotential, and the corresponding lower tendency to form bubbles.

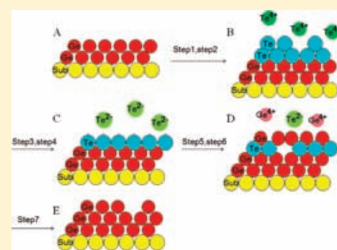

INTRODUCTION

Germanium is the other group IV semiconductor, besides silicon, and has extensive possible applications in electronics and optics.[1-3] Ge has about twice the electron mobility and four times the hole mobility of Si.[4] As Moore's law reaches the atomic limit, and scaling no longer provides solutions, there is room for material changes, possibly even the incorporation of Ge based transistors, with higher performance.[5] Owing to its low band gap, Ge is gaining popularity for used in optical and optoelectronic devices,[6-9] that is, photodetectors, waveguides, and multijunction solar cells.

A simple methodology for the formation of Ge nanofilms would greatly increase the range of possible Ge applications.[10,11] Gas phase deposition methodologies can be used for many applications, and have been applied, modified, and improved in numerous ways.[9,12-17] Attempts have also been made to form Ge films from a liquid phase, using electrodeposition as a way to avoid vacuum, high temperature, to improve structure control, achieve selective deposition, and devise a low cost deposition methodology. Because the deposition of Ge in aqueous solutions is self-limited to a few monolayers (ML),[18-21] aqueous chemistries have been avoided. A monolayer (ML) in this report corresponds to one deposited atom for each substrate surface atom. Electrochemical deposition of Ge from both ionic liquids and nonaqueous solvents [22-29] on a variety of substrates has been extensively studied. Chandrasekharan et al. performed anodic deposition of bulk Ge from K_4Ge_9 in ethylenediamine solutions.[24] Endres performed detailed studies of the electrodeposition of Ge on Au single crystal substrates in an ionic liquid (1-butyl-3 methylimidazolium-hexafluorophosphate) using a unique home-built STM design.[30,31] Endres also formed Ge nanowires and 3D-ordered macroporous Ge at bulk deposition potentials using templates.[32,33] Huang reported the deposition of bulk Ge thin films on Si substrates in 1,3-propanediol and investigated how the substrate affected deposition and crystallization.[25]

Atomic layer deposition (ALD) is the formation of materials an atomic layer at a time using surface limited reactions. Work in the authors' group has focused on the development of electrochemical atomic layer deposition (E-ALD).[34-39] Those studies have focused exclusively on the use of aqueous solutions, as the solution chemistry is well understood, ultra-high-purity water is available, waste handling is straightforward, and no glovebox is required. E-ALD involves the alternation of electrochemical surface limited reactions, in a cycle, to form nanofilms of materials. Electrochemical surface limited reactions are generally referred to as underpotential deposition (UPD), a phenomenon where an atomic layer of one element is deposited on a second at a potential prior to (under) that needed to form a bulk deposit of the element. UPD results from a negative free energy change for the formation of a surface compound or alloy. The first atomic layer of a depositing element is frequently stabilized by bonding to the substrate element. In general, E-ALD involves the use of UPD to form atomic layers of elements in a cycle. The more cycles performed, the thicker the deposit.

This report describes the development of an E-ALD cycle for the formation of Ge nanofilms, using an E-ALD cycle referred to here as "bait and switch" (B&S). The B&S concept was to form an atomic layer of one element (Ge) on a second (Te) using UPD, and then to remove the second (Te), leaving only the first (Ge) and completing one Ge deposition cycle. The cycle was then repeated to grow elemental germanium nanofilms.

EXPERIMENTAL SECTION

Deposition and cyclic voltammetry (CV) were performed using an automated flow cell deposition system[40] (Electrochemical ALD L.C., Athens, GA). The system consisted of pumps, valves, an electrochemical

Received: October 19, 2010
Published: May 03, 2011

ACS Publications © 2011 American Chemical Society

dx.doi.org/10.1021/ja109398t | *J. Am. Chem. Soc.* 2011, 133, 8199–8204

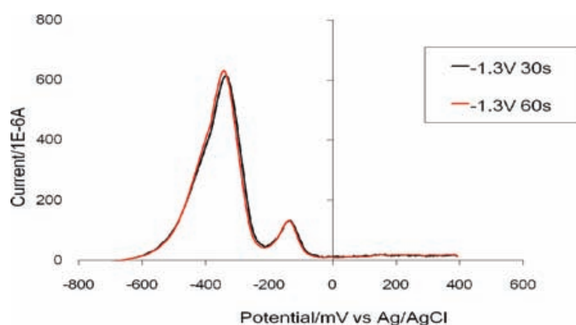

Figure 1. Oxidative stripping voltammetry of self-limited Ge deposits, formed by holding the Au substrate in the Ge solution at −1.3 V for 30 and 60 s. Both resulted in 10 mC of deposition, or about 3.5 ML, demonstrating the time independence for the self-limited Ge layer.

flow cell, and a potentiostat, all computer controlled via specialized software. Solutions, valves, and tubing were confined in a nitrogen purged Plexiglas box, to exclude oxygen. The flow cell was similar to that described in ref 40, though the auxiliary electrode has been changed from ITO to a Au wire imbedded in the cell wall opposite to the deposit area, to produce a simple primary current distribution. The reference electrode was Ag/AgCl (3 M NaCl) (Bioanalytical systems, Inc., West Lafayette, IN). The solution flow rate was 8 mL/min.

The Au substrates consisted of 300 nm thick gold films formed on glass slides, with a 10 nm Ti adhesion layer. The substrates were held at 250 °C during Au vapor deposition and then annealed at 400 °C for 12 h at 10^{-6} Torr. Cyclic voltammetry of the gold substrate in 0.1 M H_2SO_4 prior to each experiment was used to clean and check the substrate cleanliness. Cu films, 300 nm thick, were deposited by e-beam evaporation (Kurt Lesker, PVD 75), at 10^{-7} Torr, again using a 10 nm Ti adhesion layer. Cu substrates were characterized by CVs in the blank solution (0.5 M Na_2SO_4 + 50 mM $Na_2B_2O_4$, pH 9.4) prior to use.

Solutions used were 5 mM GeO_2, 0.2 mM TeO_2, and a blank. All solutions contained 0.5 M Na_2SO_4, as a supporting electrolyte, and 50 mM $Na_2B_2O_4$ as a buffer (pH 9.4). Water was supplied from a Nanopure water filtration system (Barnstead, Dubuque, IA) attached to the house DI water system. Chemicals were reagent grade or better. All solutions were purged with nitrogen before and during experiments to minimize oxygen content.

Electron probe microanalysis (EPMA) was run on a Joel 8600, wavelength dispersive scanning electron microprobe, for composition analysis. Atomic force microscopy (AFM, Molecular Imaging, PicoPlus), in intermittent contact mode, was used to characterize deposit surface morphology, using WSXM software for image processing. Surface homogeneity and morphology were investigated using a Jenavert optical metallographic microscope. A confocal Raman microscope (ThermoFisher, DXR Smart Raman Microscope), with a 532 nm laser, 10 mW power at the sample, and a 10× objective, was used to characterize deposit structure.

RESULTS AND DISCUSSION

The direct electrodeposition of Ge from aqueous solutions appears self-limited (Figure 1). Oxidative stripping of two Ge deposits formed by holding the Au substrate in the $HGeO_3^-$ ion solution at −1.3 V for 30 and 60 s, are shown in Figure 1. The curves are nearly indistinguishable, and correspond to a coverage for 3.5 ML, or 10 mC from coulometry, despite twice the deposition time. That behavior is similar to UPD, though formation of a simple surface compound is probably not the complete explanation. That 3.5 ML of deposition will be referred to simply as the self-limited deposition, given that the mechanism is not yet clear. The self-limited Ge layer was used as an Au substrate pretreatment, prior to

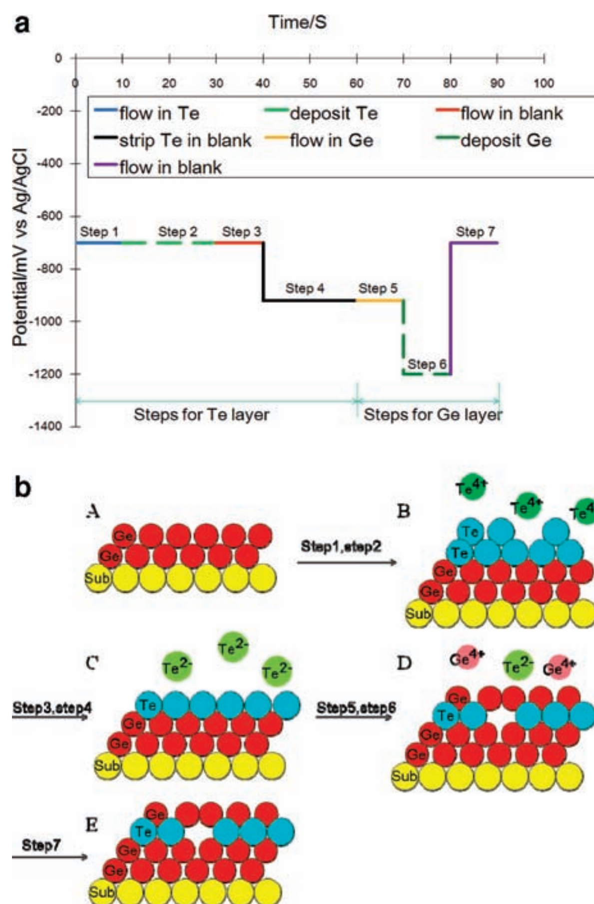

Figure 2. (a) An example of a Ge_xTe_y E-ALD deposition cycle. Solid lines indicate flowing solutions, while dashed lines indicate stagnant solutions. (b) A scheme for one E-ALD cycle of Ge_xTe_y deposition. As noted in the text, E-ALD deposits were formed after initial formation of the self-limiting Ge layer (Figure 1), represented by two atomic layers of Ge on the initial Au substrate. Note in schematic D that some Te^{2-} was formed, and lost, during the deposition of Ge.

E-ALD. A more detailed study of self-limited Ge deposition was previously reported by this group.[18]

In a recent study developing an E-ALD cycle to form Ge_xTe_y and $Ge_xTe_ySb_z$, phase change materials, Ge-rich films of Ge_xTe_y, were formed.[41] Figure 2a is a Ge_xTe_y deposition cycle (solid lines indicate flowing solutions, while dashed lines indicate stagnant solutions), and Figure 2b is a scheme for the cycle. Frames A−C (Figure 2b) are formation of an Te atomic layer on Ge, while frames D−E are formation of an atomic layer of Ge on Te. An atomic layer (AL) is no more than one atom thick, with a coverage less than a ML. The Te AL formation involved initial deposition of a little over a ML (Figure 2a, steps 1 and 2), followed by reductive stripping of weakly bound (bulk) Te atoms, in flowing blank solution at −0.92 V (Figure 2a, steps 3 and 4), resulting a AL of strongly held Te, stabilized by bonding with Ge. Ge UPD (Figure 2a, steps 5 and 6) on Te is diagramed in Figure 2b, steps C and D. Figure 2b suggests that Ge AL formation is accompanied by the loss of some Te. A blank solution was flushed through the cell in Figure 2a, step 7, removing excess $HGeO_3^-$ ions and completing one Ge_xTe_y deposition cycle. Nanofilms of Ge_xTe_y were formed by repeating the cycle.[41]

Figure 3 displays Ge and Te coverages, as well as the Ge/Te ratios, for a sequence of Ge_xTe_y deposits as a function of the

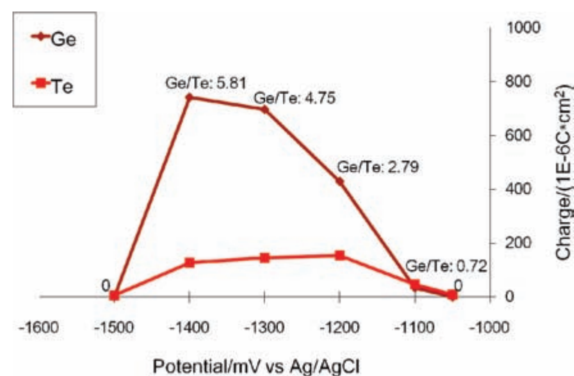

Figure 3. Ge and Te coverages/cycle, as a function of the Ge deposition potential, as well as Ge/Te ratios. Coverages were determined from oxidative stripping coulometry for Ge and Te. All deposits were formed using the E-ALD cycle diagramed in Figure 2.

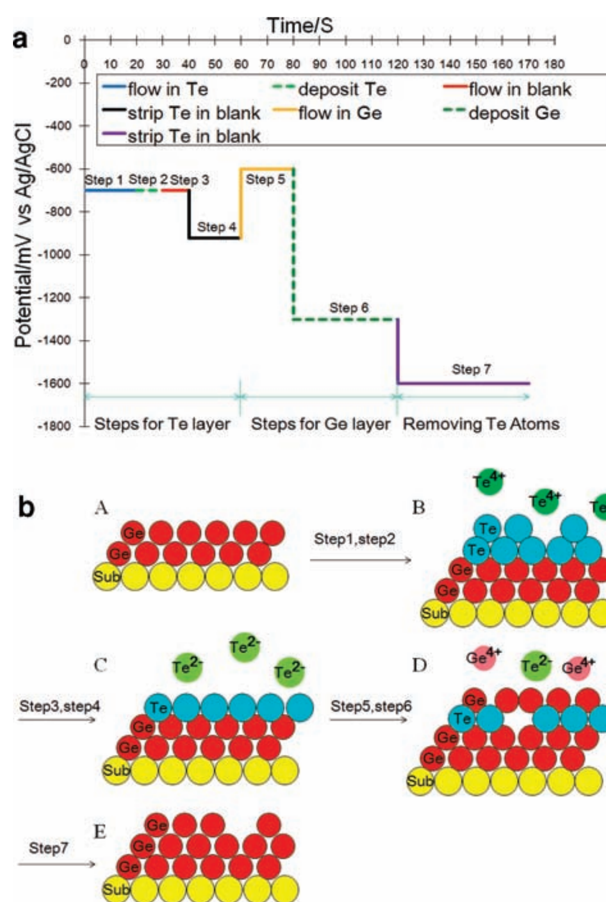

Figure 4. (a) An example of a B&S cycle, used to form Ge nanofilms. Solid lines indicate flowing solutions, while dashed lines stand for stagnant solutions. (b) A scheme for one B&S Ge E-ALD cycle. The cycle steps from panel a are noted.

potential used for Ge deposition. The E-ALD cycle outlined in Figure 2 was used for each deposit, varying only the Ge deposition potential (step 6, Figure 2). More Ge deposited, the more negative the potential, and the Ge/Te also increased. By −1.5 V, the potential was so negative that neither Ge nor Te was deposited, as even strongly bound Te atoms were reduced to Te^{2-} ions. No Te atoms, no Ge atoms deposited. Ge and Te

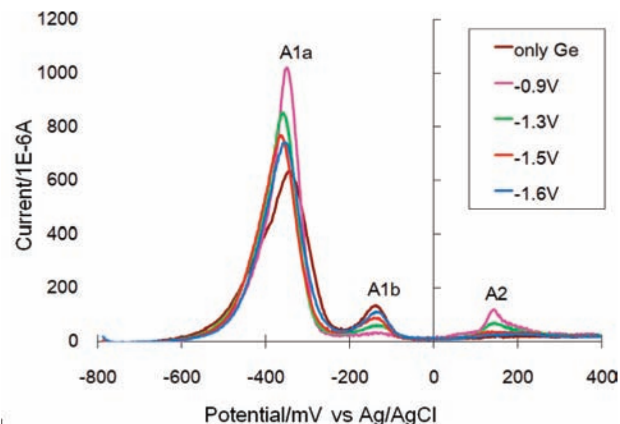

Figure 5. Oxidative stripping voltammetry from surfaces where the Te reductive stripping potential (step 4, Figure 4a) was varied. The smaller peak A1b is, the more Te is on the surface, since the presences of Te prevents Ge from binding to the Au substrate, and peak A1b is oxidation of a Ge AL in contact with Au. Coulometry from peak A2 is a measure of the total Te coverage.

coverages/cycle (Figure 3) were determined using coulometry for deposit oxidative stripping. It was found most consistent to take the difference between deposits formed with 5 cycles and 10 cycles, and then divide by 5. This served to minimize the importance of the 10 mC of charge for the initially formed self-limited Ge layer. The oxidative stripping peaks for Ge and Te were well separated, allowing accurate coulometry.[41] The validity of the Ge/Te ratios was supported by EPMA for thicker films, formed using the same Ge deposition potentials.[41]

Those previous studies of E-ALD cycles for Ge_xTe_y, indicated a wide range of Ge/Te ratios could be formed (Figure 3), suggesting Te might be reductively stripped from thin Ge_xTe_y deposits each cycle to leave only Ge.[41] That is, nanolayers of Ge_xTe_y subjected to reduction at relatively negative potentials produced telluride ions, stripping the deposit of Te, and leaving Ge, suggesting the B&S E-ALD cycle: Ge AL baited to deposit on a Te AL, and then switching out the Te AL by reductive stripping to leave the Ge AL.

Figure 4a is a potential time diagram for a Ge B&S E-ALD cycle, and Figure 4b is a corresponding scheme. The B&S cycle studies, for each deposit, began with the self-limited deposition of Ge on the substrate, on which the E-ALD cycles were performed. The cycle in Figure 4a is similar to that used to form Ge_xTe_y (Figure 2), except that the potential used in step 7 has been shifted negative to reductively strip Te atoms from the Ge_xTe_y layer (Figure 4b, schematics D and E), leaving only Ge.

Initial studies to optimize the Ge B&S cycle examined the potential used to reduce Te from the Ge surface. A Te layer, slightly in excess of a ML (Figure 4a, steps 1−3, Figure 4b, schematics A and B), was first formed on the self-limited Ge layer. A sequence of different potentials were used to strip the weakly bound Te (Figure 4b, C), with blank solution flowing, for 30 s. Oxidative stripping of the self-limited Ge layer, and any Te remaining, was performed in a scan from −0.8 to 0.4 V (Figure 5). Peak A1a corresponds to bulk Ge oxidation, peak A1b corresponds to oxidation of Ge bound to the Au surface,[18] and Peak A2 corresponds to oxidation of Te.[41]

The brown line in Figure 5 was from a self-limited Ge layer and no Te. Peak A1a, appears smaller than the rest, but the total Ge coverage from coulometry (peaks A1a + A1b) was about the

same in each scans in Figure 5. Te, if present, bound strongly to the Au surface, covering it and preventing Ge adsorption on the Au. As noted, A1b is the oxidation of Ge bound to Au, and thus is largest when no Te is present. With no Te present for the brown line, peak A1b was full sized. In a previous study of Ge deposition on a Au(111) single crystal, peak A1b corresponded to oxidation of a $^4/_9$ths ML coverage Au(111)(3 × 3)-Ge structure, to form $HGeO_3^-$ ions.[18] In scans where Te was present, peak A2 varied, a function of the reductive Te striping potential used, and the amount of Te left on the surface. The pink line was after Te reductive stripping at −0.9 V, where peak A1b was nearly absent, while peak A2 displayed a maximum Te coverage.[34,42−44] Te appeared to destabilize Ge bound to Au, so that it oxidized with the bulk Ge, in peak Peak A1a. The more negative was the potential used for reductive Te stripping, (Figure 4, step 4) the less Te was present, the more Ge was bound to Au and the larger was the peak A1b. Overall, the data in Figure 5 suggested a Te reduction potential below −1.6 V results in complete stripping of Te from the Ge (step 4).

To investigate the Ge coverage dependence of Te AL coverage, again deposits were formed starting with the self-limited Ge layer, followed by steps 1−4 (Figure 4). The Te reductive stripping potential was varied, adjusting the Te AL coverage. A Ge AL was then deposited using the same conditions in Figure 4, steps 5 and 6. The resulting deposits were oxidatively stripped by scanning from −0.8 to 0.4 V. Those results indicated that higher Te AL coverages resulted in higher Ge coverages, consistent with having more Te atoms to bond with. However, it was not one Ge for one Te, as the Ge/Te ratio increased with the Te AL coverage. It appears that as the Te AL coverage goes up, the extra Te atoms bind with a higher number of Ge atoms. This suggests that higher Te AL coverages result in more weakly bound Te atoms, in addition to the strongly bound. Apparently, less strongly bound Te atoms bond more readily Ge atoms, coordinating with a higher stoichiometry, and raising the Ge/Te ratio, than do strongly bound Te atoms. The strongly bound Te could be thought of as more coordinatively saturated, than the weakly, and thus less able to bond subsequent Ge.

Other observations made while developing the B&S cycle for Ge include the following: (1) Some Ge appears to be removed from the surface during reductive Te stripping, step 7 (Figure 4a). According to the Pourbaix diagram, it may be possibly to form a soluble GeH_4 species by electrochemical reduction, though no clear evidence of such a reaction has been noted by this group.[18,45] It is more likely that during Te stripping some particles of Ge became detached and were lost. (2) It has been shown that multiple small potential shifts during step 6, for Ge deposition (Figure 4a), instead of a single shift, resulted in a higher Ge coverage. This appears to result from the convolution of the kinetics for Ge deposition and Te stripping, with their respective surface coverages, during the Ge deposition step. In general, more Ge was deposited as the more negative was the potential step used for Ge deposition, for a single potential shift. On the other hand, when a less negative potential was used for Ge deposition, less Ge was deposited, but more Te remained on the surface; less Te was stripped. When a second, more negative, potential shift was applied, more Ge was deposited than would have been deposited in a single shift, because some of the Te which would have stripped had been stabilized by coordination with Ge, facilitating more Ge deposition. The suggestion was made by one of this papers reviewers, that use of a linear scan might be the optimal procedure for this step, and the authors agree.

The Ge films formed on Au were not homogeneous. There were macroscopic areas where no deposit was visible by eye. The most likely reason for the heterogeneity was that hydrogen

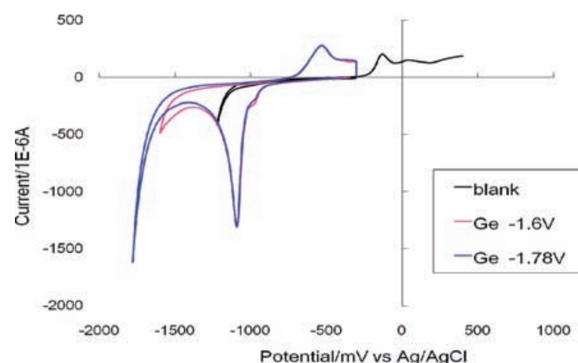

Figure 6. Cyclic voltammetry for a Cu substrate. The black line was a CV in the blank solution (0.5 M Na_2SO_4 + 50 mM $Na_2B_2O_4$, pH 9.40). The pink and blue lines were for CVs in the $HGeO_3^-$ solution (0.5 M Na_2SO_4 + 50 mM $Na_2B_2O_4$ + 5 mM GeO_2, pH 9.40). The electrode area was 3.3 cm^2, and the scan rate was 10 mV/s.

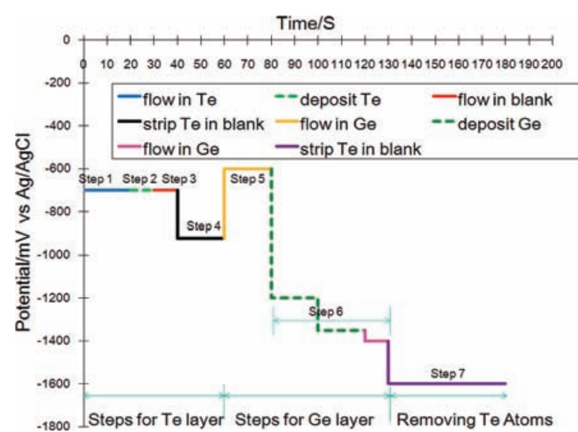

Figure 7. An example of a modified Ge E-ALD cycle used on Cu substrates. Solid lines are flowing solutions, while dashed lines are stagnant.

bubbles, generated at the low potentials used in this study, were interfering with the deposit growth. The hydrogen overpotential on Au is very low, so that any Au in contact with the solution, at the negative potentials needed for Ge deposition (Figure 4a), would result in significant hydrogen evolution and bubble formation. Bubbles were evident in the electrochemical flow cell and had to be persuaded to leave by tapping the cell while solution was flowing.

To investigate the issue of bubbles blocking the surface, Cu substrates were used, as Cu has a much greater hydrogen overpotential, which greatly limits bubble formation. The resulting Ge films were visually homogeneous, compared with those formed on Au substrates. With both Au and Cu substrates, extensive hydrogen evolution damaged the thin, 200−300 nm, metal films used as substrates.

The black line in Figure 6 was a Cu CV in the blank solution. The pink and purple lines in Figure 6 are Cu CVs in the $HGeO_3^-$ solution, scanned to −1.6 and −1.78 V, respectively. Ge deposition is evident as the reduction peak at −1.09 V, corresponding to 7.7 mC of Ge, or about 2.7 ML. The peak appears self-limited, as it was for Ge deposition on Au, though the coverage was slightly less. Deposits on Cu substrates were again begun with the self-limited Ge layer, by holding at −1.3 V for 30 s in the $HGeO_3^-$ solution. Subsequent Ge growth was performed

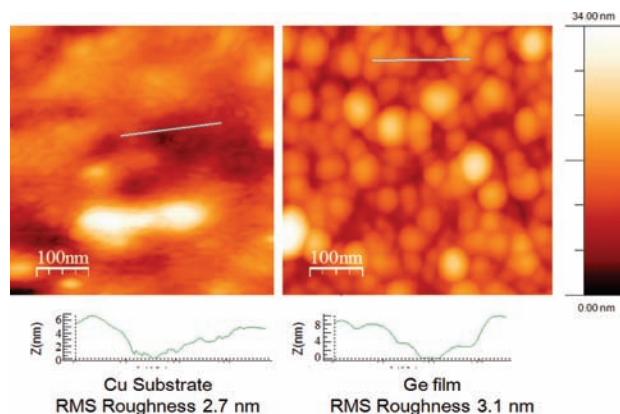

Figure 8. AFM images of a Cu substrate and an as-deposited Ge film deposited on that Cu substrate.

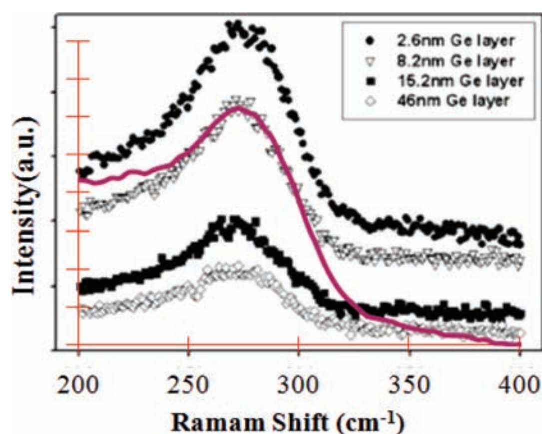

Figure 9. Raman spectra of as deposited Ge nanofilom (purple line) superimposed on literature data.[46]

using the E-ALD cycle diagramed in Figure 7, for which multiple potential shifts were used for Ge deposition (step 6).

Figure 8 displays AFM images of a Cu substrate, and an as-deposited Ge film formed on top using 50 B&S cycles (Figure 7). The Ge deposit was homogeneous, and covered the whole surface with 50 nm crystallites. The rms roughness of the Ge film was close to that for the roughness of the Cu substrate, Figure 8, though there were obvious differences in morphology. The tops of the Ge grains look rounded, like a ball. However, aspect ratios tend to be distorted in AFM, where x and y are 500 nm full scale, and z is listed as 34 nm.

EPMA of deposits indicated that the Te atomic % was below the detection limit, about 0.2 atomic % (based on all elements detected: Au or Cu, Ge and Te). It was probably closer to 1%, relative to the Ge film itself. Measurements of Ge atomic % across the deposit were homogeneous. Figure 9 shows the Raman spectrum for the as deposited film superimposed on amorphous Ge Raman spectra measured by Eunice.[46] The Raman peak shape and shift indicate a close match with literature spectra for amorphous Ge.[46,47]

CONCLUSION

Ge films were electrochemically deposited from aqueous solutions using E-ALD. A new type of surface limited reaction, or cycle, was developed and is referred to here as bait and switch (B&S). The cycle involved deposition of a Te AL (as bait), and then Ge UPD on the Te AL. Once the Ge AL was formed, the Te AL was reductively stripped (switched out), leaving only Ge behind. These studies were an outgrowth of the development of an E-ALD cycle for Ge_xTe_y nanofilm formation, a phase change material. It was observed in the Ge_xTe_y studies that a high Ge/Te ratio could be produced. In the present studies, it was found that more homogeneous Ge deposits were formed on Cu substrates, than on Au, due to the higher hydrogen overpotential compared with Au. The higher overpotential suppressed hydrogen bubble formation at the negative potentials needed to deposit Ge, allowing homogeneous deposits to form. The resulting Ge deposits covered the Cu surface with 50 nm amorphous Ge grains. No pattern was observed using grazing incidence XRD, consistent with an amorphous deposit, and a good match was observed with literature Raman spectra for amorphous Ge. The deposits were clearly not single crystal quality nor possibly those formed electrochemically from ionic liquids. They were, however, an indication that Ge can be formed electrochemically from aqueous solution, and they represent an excellent starting point for subsequent investigations of the variables controlling structure in Ge deposition via E-ALD.

AUTHOR INFORMATION

Corresponding Author
stickney@chem.uga.edu

ACKNOWLEDGMENT

Support from the National Science Foundation, Division of Materials Research, is gratefully acknowledged.

REFERENCES

(1) Patel, N.; Ramesha, A.; Mahapatra, S. *Microelectron. J.* **2008**, *39*, 1671–1677.
(2) Tsybeskov, L.; Lockwood, D. J. *Proc. IEEE* **2009**, *97*, 1284–1303.
(3) King, T. J.; Saraswat, K. C. *J. Electrochem. Soc.* **1994**, *141*, 2235–2241.
(4) Kamata, Y. *Mater. Today* **2008**, *11*, 30–38.
(5) Shang, H.; Frank, M. M.; Gusev, E. P.; Chu, J. O.; Bedell, S. W.; Guarini, K. W.; Ieong, M. *IBM J. Res. Dev.* **2006**, *50*, 377–386.
(6) Solomon, A.; Fengnian, X.; Stephen, W. B.; Ying, Z.; Teya, T.; Philip, M. R.; Yurii, A. V. In *Optical Fiber Communication Conference*; Optical Society of America: Washington, DC, 2009; p 1−3.
(7) King, R. R.; Law, D. C.; Edmondson, K. M.; Fetzer, C. M.; Kinsey, G. S.; Yoon, H.; Sherif, R. A.; Karam, N. H. *Appl. Phys. Lett.* **2007**, *90*, 183516.
(8) Tang, L.; Kocabas, S. E.; Latif, S.; Okyay, A. K.; Ly-Gagnon, D.-S.; Saraswat, K. C.; Miller, D. A. B. *Nat. Photon.* **2008**, *2*, 226–229.
(9) Oehme, M.; Werner, J.; Kaschel, M.; Kirfel, O.; Kasper, E. *Thin Solid Films* **2008**, *517*, 137–139.
(10) Lee, H.; Lee, D. H.; Kanashima, T.; Okuyama, M. *Appl. Surf. Sci.* **2008**, *254*, 6932–6936.
(11) Yang, M.; Wu, R. Q.; Chen, Q.; Deng, W. S.; Feng, Y. P.; Chai, J. W.; Pan, J. S.; Wang, S. J. *Appl. Phys. Lett.* **2009**, *94*, 142903–142903-3.
(12) Cole, J. J.; Lin, E.-C.; Barry, C. R.; Jacobs, H. O. *Small* **2010**, *6*, 1117–1124.
(13) Tsao, C. Y.; Weber, J. W.; Campbell, P.; Widenborg, P. I.; Song, D. Y.; Green, M. A. *Appl. Surf. Sci.* **2009**, *255*, 7028–7035.
(14) Alonso, M. I.; Garriga, M.; Bernardi, A.; Goni, A. R.; Lopeandia, A. F.; Garcia, G.; Rodriguez-Viejo, J.; Labar, U. *Thin Solid Films* **2008**, *516*, 4277–4281.

(15) Choi, D.; Ge, Y.; Harris, J. S.; Cagnon, J.; Stemmer, S. *J. Cryst. Growth* **2008**, *310*, 4273–4279.
(16) Masarotto, L.; Yckache, K.; Fanton, A.; Aussenac, F.; Fillot, F. *Thin Solid Films* **2010**, *518*, 5382–5386.
(17) Yamamoto, M.; Hanna, J.; Miyauchi, M. *Appl. Phys. Lett.* **1993**, *63*, 2508–2510.
(18) Liang, X. H.; Kim, Y. G.; Gebergziabiher, D. K.; Stickney, J. L. *Langmuir* **2010**, *26*, 2877–2884.
(19) Jayakrishnan, S.; Pushpavanam, M.; Shenoi, B. A. *Surf. Technol.* **1981**, *13*, 225–240.
(20) Fink, C. G.; Dokras, V. M. *J. Electrochem. Soc.* **1949**, *95*, 80–97.
(21) Freyland, W.; Zell, C. A.; El Abedin, S. Z.; Endres, F. *Electrochim. Acta* **2003**, *48*, 3053–3061.
(22) Al-Salman, R.; Abedin, S. Z.; Endres, F. *Phys. Chem. Chem. Phys.* **2008**, *10*, 4650–4657.
(23) Saitou, M.; Sakae, K.; Oshikawa, W. *Surf. Coat. Technol.* **2003**, *162*, 101–105.
(24) Chandrasekharan, N.; Sevov, S. C. *J. Electrochem. Soc.* **2010**, *157*, C140–C145.
(25) Huang, Q.; Bedell, S. W.; Saenger, K. L.; Copel, M.; Deligianni, H.; Romankiw, L. T. *Electrochem. Solid State Lett.* **2007**, *10*, D124–D126.
(26) Huang, Q.; Deligianni, H.; Romankiw, L. T. *Electrochem. Solid State Lett.* **2007**, *10*, D121–D123.
(27) Endres, F. *Phys. Chem. Chem. Phys.* **2001**, *3*, 3165–3174.
(28) Endres, F.; El Abedin, S. Z. *Chem. Commun.* **2002**, 892–893.
(29) Mukhopadhyay, I.; Freyland, W. *Chem. Phys. Lett.* **2003**, *377*, 223–228.
(30) Endres, F.; El Abedin, S. Z. *Phys. Chem. Chem. Phys.* **2002**, *4*, 1649–1657.
(31) Endres, F.; El Abedin, S. Z. *Phys. Chem. Chem. Phys.* **2002**, *4*, 1640–1648.
(32) Al-Salman, R.; Mallet, J.; Molinari, M.; Fricoteaux, P.; Martineau, F.; Troyon, M.; El Abedin, S. Z.; Endres, F. *Phys. Chem. Chem. Phys.* **2008**, *10*, 6233–6237.
(33) Meng, X. D.; Al-Salman, R.; Zhao, J. P.; Borissenko, N.; Li, Y.; Endres, F. *Angew. Chem., Int. Ed.* **2009**, *48*, 2703–2707.
(34) Banga, D. O.; Vaidyanathan, R.; Liang, X. H.; Stickney, J. L.; Cox, S.; Happeck, U.; Pergamon-Elsevier Science Ltd: Oxford, U.K., 2008; p 6988—6994.
(35) Kim, J. Y.; Kim, Y. G.; Stickney, J. L. *J. Electrochem. Soc.* **2007**, *154*, D260–D266.
(36) Thambidurai, C.; Kim, Y. G.; Jayaraju, N.; Venkatasamy, V.; Stickney, J. L. *J. Electrochem. Soc.* **2009**, *156*, D261–D268.
(37) Muthuvel, M.; Stickney, J. L. *Langmuir* **2006**, *22*, 5504–5508.
(38) Vaidyanathan, R.; Cox, S. M.; Happek, U.; Banga, D.; Mathe, M. K.; Stickney, J. L. *Langmuir* **2006**, *22*, 10590–10595.
(39) Oznuluer, T.; Demir, U. *J. Electroanal. Chem.* **2002**, *529*, 34–42.
(40) Flowers, B. H.; Wade, T. L.; Garvey, J. W.; Lay, M.; Happek, U.; Stickney, J. L. *J. Electroanal. Chem.* **2002**, *524—525*, 273–285.
(41) Liang, X.; Jayaraju, N.; Thambidurai, C.; Zhang, Q.; Stickney, J. L. *Chem. Mater.* **2011**, *23*, 1742–1752.
(42) Lay, M. D.; Stickney, J. L. *J. Electrochem. Soc.* **2004**, *151*, C431–C435.
(43) Sorenson, T. A.; Suggs, D. W.; Nandhakumar, I.; Stickney, J. L. *J. Electroanal. Chem.* **1999**, *467*, 270–281.
(44) Sorenson, T. A.; Varazo, K.; Suggs, D. W.; Stickney, J. L. *Surf. Sci.* **2001**, *470*, 197–214.
(45) Pourbaix, M. *Atlas of Electrochemical Equilibira in Aqueous Solution*; Pergamon Press: New York, 1966.
(46) Goh, E. S. M.; Chen, T. P.; Sun, C. Q.; Liu, Y. C. *J. Appl. Phys.* **2010**, 107.
(47) Kuo, C. C. *J. Russ. Laser Res.* **2008**, *29*, 167–175.